Membrane Emulsification using Membranes of Regular Pore Spacing: Droplet Size and Uniformity in the Presence of Surface Shear

Emanuela Egidi[1], Gilda Gasparini[1], Richard G. Holdich[1*], Goran T. Vladisavljević[1]. and Serguei R. Kosvintsev[2]
[1]Department of Chemical Engineering, Loughborough University, Leicestershire, LE11 3TU, U.K.
[2]Micropore Technologies LTD, Epinal Way, Loughborough, Leics., LE11 3EH.

Abstract

During membrane emulsification it is shown that the size of the drops formed at the membrane surface may increase with increasing dispersed phase injection rate through the membrane, or it may decrease, depending on the prevailing conditions. This is illustrated using a stirrer positioned above a flat disc membrane with a regular array of pores of 20 μm diameter and a spacing between the pores of 80 μm and another membrane of 200 μm pore spacing. In the former case an additional mechanism for drop detachment is the push-off force, which is determined by the geometry of the drops as they deform at the membrane surface. In the force balance, the push-off force may be added to the shear-drag force to cause drop detachment. In the case of the 200 μm pore spaced membrane this force is much less prominent. The capillary-shear model has been modified to include this push-off force. The study required the use of very low dispersed phase injection rates and very high rates. Hence, two different types of pumps were used to provide these: a peristaltic and syringe pumps. A small study comparing the drop size, and size distributions, showed that the pump type did not influence the drops produced by the membrane emulsification process.

keywords
emulsification, stirred cell, sieve-membrane, force balance, push-off force

*corresponding author's address:
Professor Richard Holdich, Department of Chemical Engineering, Loughborough University, Loughborough, Leicestershire, LE11 3TU, UK. Tel: +44 1509 222519, Fax: +44 1509 223923, e-mail: r.g.holdich@Lboro.ac.uk

Introduction

Emulsions have an important role in the pharmaceutical, petrochemical, cosmetic and food industries. Emulsions are conventionally prepared using stirred tanks, high pressure homogenizers and rotor stator devices such as colloid mills and static mixers. These methods have a number of problems, such as: unreliable scale-up, wide particle size distribution produced, high mechanical stress due to fluctuating forces in the flow field and poor batch to batch reproducibility [1,2]. Membrane emulsification overcomes many of these problems and is a method that has received increasing attention over the last 15 years. Initially, work was performed in Japan using the Shirasu porous glass membranes, and many potential applications have been documented [3]. In this process, the dispersed phase is passed through the pores of a membrane, where the droplets are formed at the interface between the membrane and the continuous phase. Membrane emulsification has many advantages over conventional methods of dispersion generation, such as low shear stress, and consequent reduction in energy requirement (especially for producing small droplets), simplicity of design, consistent product and smaller amount of surfactant required [4]. When using membrane emulsification technology, the most important advantage is the possibility to produce droplets of a defined size with a narrow size distribution. The size of the emulsion droplets is determined by various process parameters including the membrane properties of: pore size, distance between the pores, pore shape and membrane wettability by the liquids present; together with process conditions of: shear stress at the membrane surface, discontinuous (i.e. injected) phase flux, viscosity of the phases and interfacial tension [5, 6, 7]. To form the droplets and to prevent them from coalescing, a shear field is used. In cross-flow membrane emulsification, shear stress is generated at the membrane/continuous phase interface

by recirculation of the continuous phase using a pump. This recirculation may induce breakage of the droplets inside the pipes and pump. One solution to this problem is to use a rotating membrane [8], where the shear stress is developed by rotating the membrane rather than using a flowing continuous phase. In other devices, the shear at the membrane surface was provided by a magnetic stirrer or membrane vibration [9]. In this study a membrane emulsification Dispersion Cell has been investigated. It contains a circular disc membrane positioned below a simple paddle stirrer, which induces shear at the membrane surface. As showed in [5], the shear profile provided by the paddle stirrer is not uniform, but it produces monosized emulsions because most of the drop generation takes place around the critical radius where the shear field is at a maximum.

There are two main detachment mechanisms described in the literature: spontaneous transformation–based (STB) droplet formation [10, 11] and, shear induced droplet formation [12, 13]. STB describes situations where the droplets are formed predominantly in the absence of shear. In silicon microgrooved devices, the droplets deform and detach from the microsubstrate as a result of the geometry, not because of the imposed shear stress, or contacts between themselves [10]. Rayner at. al [11] employing the Surface Evolver software, used the change in interfacial energy to model the droplet shape and hence size. Shear induced droplet formation describes the condition where the shear stress affects the size and distribution of the droplets. It has been modelled using an algebraic torque balance equation (TBE) and a force balance (FBE) along the droplet contact line located around the membrane pore border [12-15]. During the detachment process, a number of forces have been identified; it has been shown that for micron scale droplets the inertia and buoyancy forces are

approximately 9 and 6 orders of magnitude smaller, respectively, than the drag due to shear at the membrane surface and therefore can be neglected in the force balance type models [12, 14].

In addition to shear stress, the rate at which the dispersed phase is passed through the membrane plays a crucial role. If dispersed phase flux is increased, the droplet volume prior to detachment increases, hence the droplet size increases [15, 16, 17]. Another phenomenon linked to the dispersed phase flux is the change in dynamic interfacial tension [12]. The interfacial tension is increased by the creation of fresh interface as the droplet expands and lowers the surfactant coverage per unit area. This is a kinetic process, as the interfacial tension will be lowered by new surfactant adsorbing from the continuous phase to the surface, but the faster the dispersed phase flux the lower will be the overall effective surfactant concentration during drop formation at the interface between the two phases. Lastly the increase in injection rate leads to a higher number of active pores and may cause a transition from a dripping regime to a continuous outflow regime. Vladisavljević et. al. [17] using a microscope video system and an SPG membrane with 15 μm diameter pores, showed that even if droplets formed at the same time at adjacent pores and contacted each other, there was no coalescence, in the system studied.

There are a number of references for the description of drop formation, they mostly consider a single drop, not the drop interactions. Abrahamse et al. [18], studied the interaction during cross-flow emulsification using a microsieve consisting of uniform micron sized pores. By the use of video and a microscope, they showed that droplets forming at pores sometimes touched each other while they were growing. Due to this

steric interference, droplets detached. Because of the small number of pores in the membrane used, and some surface coalescence, the force due to droplet 'push-off' in this case led to a high degree of drop size polydispersity. Zhu et. al. [9] used stationary and vibrating micromachined membranes with a pore diameter of 2.5 μm and distance between the pores ranging from 20 to 100 μm. They found that the droplet size increased with increasing the dispersed phase flow rate up to a maximum and then decreased when the pore distance was at the finer end of the pore spacing range. By video-microscopy, it was found that as the droplets grew in size, they interact and appeared to create a push-off on the nearby drops which contributed to droplet detachment. In this case coalescence was not observed, as confirmed elsewhere [17]. Moreover, they hypothesized that an optimum inter-pore distance can facilitate droplet detachment.

An algebraic equation for the force due to neighbouring drops, i.e. push-off, was shown when no shear is applied [7]. Briefly, for a membrane with a regular array of pores, if the drop diameter is bigger than the distance between the pores, the drop shape deviates from spherical towards a spheroid when at high dispersed phase flux. Deformation of the drop shape from the minimum energetic state leads to additional work done in the system. The drop size predictive equation is based on the concept that work done on the system goes into increasing the interfacial area between the emerging drop and the continuous phase, until the force on the drop is sufficient to overcome the capillary force holding the drop to the membrane opening.

The present work reported here extends the earlier work [7] as shear is now included in the predictive model, together with a comparison of the effects due to the different

phenomena taking place at the drop-continuous phase interface, and how they influence the resulting drop size. A range of dispersed phase fluxes and shear stresses at the membrane surface have been tested on membranes with different pore spacings to investigate the push-off effect.

Model for the prediction of droplet diameter

As reported in many previous papers [11,15,19] there are a number of forces acting on a growing droplet from a porous membrane. Of all these forces, the capillary force, F_{Ca}, and an opposing drag force, F_D, are the most important. For the droplet size produced, the buoyancy force does not significantly influence the force balance.

The droplet diameter can be predicted based on a simple force balance. The expression for the capillary force can be modified to consider the neck, which exists between the forming drop and the membrane pore, by introducing another force called Static force, F_{stat} [19,20]. As shown by Xu et al. [20], there is a static pressure difference due to pressure between the inside and outside of the droplet which can be expressed as

$$F_{stat} = \frac{4\gamma}{d_d}\frac{\pi}{4}d_p^2 \quad (1)$$

where the neck diameter is approximated to the membrane pore diameter, (d_p), γ is the interfacial tension and d_d is the droplet diameter. The force due to interfacial tension (capillary force) is

$$F_{Ca} = \pi d_p \gamma \quad (2)$$

It is possible to modify the capillary force in order to consider the neck

$$F_{Ca} - F_{stat} = \pi d_p \gamma \left(1 - \frac{d_p}{d_d}\right) \tag{3}$$

When the droplets are in a region close to the pore diameter, the expression considering the neck underestimates the net capillary force, and the correction for this neck static pressure is no longer applicable. In such cases it is preferable to use the uncorrected expression, equation (2). The expression for the drag force is based on Stokes's drag expression, with a correction factor (k_{Wl}) to consider the effect of the nearby walls in the motion of a droplet, as reported in [21]. For the system reported here k_{Wl} is 3.4926

$$F_D = 3\pi k_{wl} \eta_{cont} v d_d \tag{4}$$

where v is the relative velocity between the drop and the continuous phase and η_{cont} is the viscosity of the continuous phase

$$v = \omega r_{trans} \left(1 - \exp\left(-\frac{d_d}{2\delta}\right)\right) \tag{5}$$

ω is the rotation speed of the paddle stirrer, δ is the boundary layer thickness as can be predicted by the Landau-Lifshitz. equation

$$\delta = \sqrt{\frac{\eta_{cont}}{\rho_{cont}\omega}} \tag{6}$$

where ρ_{cont} is the density of the continuous phase. The transitional radius between the free and forced vortex for the stirred system is given by the following expression

$$r_{trans} = \frac{D}{2} \cdot 1.23 \left(0.57 + 0.35 \cdot \frac{D}{T} \right) \left(\frac{b}{T} \right)^{0.036} n_b^{\,0.116} \frac{\mathrm{Re}}{1000 + 1.43\,\mathrm{Re}} \qquad (7)$$

where D=3.1 cm is the paddle width, T=3.5 cm is the vessel width, b=1.2 cm is the paddle stirrer width ~~where *D* is the paddle width, *T* is the vessel width, *b* is the paddle stirrer height above the membrane~~ and n_b is the number of blades of the paddle. The rotational Reynolds number is

$$\mathrm{Re} = \frac{\rho_{cont} \omega D^2}{2\pi\eta_{cont}} \qquad (8)$$

The expression for the velocity considers the boundary layer, equation (5), at the membrane surface, see Figure 1(a) and (b) for an illustration of the Dispersion Cell and the transitional radius. In figure 1b the shear pattern is represented too. The shear on the membrane surface increase linearly moving from the centre towards the edges, it reaches a maximum at the transitional radius distance and then it decreases exponentially in the forced vortex region. As assumed in [5], the annular area corresponding to the transitional radius is the most active from the point of view of droplets generation. The higher shear leads to an early detachment of the droplets, the pressure in that region is lower and the oil phase is mainly pushed through this part. Experiments with only the annular area working were performed in [6]. The droplets obtained with a fully working membrane and a ring one have the same size, those one obtained with the latter are more monosized. This proves that even in a fully working membrane, the annular ring, hence the maximum shear value is mainly responsible for

the droplet size. The force balance, using equations (3) or (2) together with equation (4) gives the droplet diameter in the absence of any push-off force.

As noted also by [7, 9, 18], when droplets are able to touch, and they are stable enough not to coalesce, another factor becomes important and it has been referred to as the push-off force. This was derived previously as [7]:

$$F_{push-off} = \frac{1}{2}\frac{\gamma\pi d_d^3 L \cdot \arcsin\left(\frac{\sqrt{d_d^6 - L^6}}{d_d^3}\right)\left(d_d^6 - 2L^6\right)}{\left(d_d^6 - L^6\right)^{3/2}} + \frac{\gamma\pi d_d^2 L^7}{2\left(d_d^6 - L^6\right)\sqrt{\frac{L^6}{d_d^2}}} - \frac{2\gamma\pi L^2}{3d_d} \qquad (9)$$

where L is the pore spacing. Therefore, when taking into account the effect of the adjacent droplets, the force balance to solve is given by combining equations (3) or (2), together with (4) and (9)

$$F_{Ca} - F_{stat} = F_D + F_{push-off} \qquad (10)$$

In all the following work equation (3) was used in preference to equation (2) as the drop size was significantly bigger than the pore diameter. The existence of drop diameter in so many of the constituent equations led to the need for a numerical solution to equation (10). For this, Maple (v11) was used.

Materials and Methods

The emulsion was obtained by a membrane technique using a stirred cell with a flat metal disc membrane under the paddle blade stirrer, see Figure 1, which was supplied by Micropore Technologies Ltd (Loughborough, UK). The two membranes used had different distances between the pores of: 80 and 200 μm and same pore size of 20 μm. Based on these characteristics, the porosity is 5.6% and 0.9% respectively and the

number of pores is more than 788,000 for the first and around 126,000 for the latter. The discontinuous phase was made of sunflower oil (food grade from a local supermarket). The continuous phase was composed of 2% Tween 20 (polyoxylethylene sorbitan monolaureate from Fluka, UK) in reverse osmosis water (obtained from a Millipore RO unit). A total of 10 ml of discontinuous phase was injected through the membrane into 150 ml of continuous phase for each test. The emulsion is obtained by injecting the discontinuous phase through a disc membrane with a regular array of pores, see Figure 1(d), into the continuous phase, agitated by the paddle blade stirrer which provides the shear at the membrane surface.

Two types of pumps were required to cover the wide range of injection rates tested: the syringe pump provided flows as low as 0.1 ml/min whereas the peristaltic pump was used for the higher flow rates. The peristaltic pump was a Watson Marlow model 101 and the syringe pump was a Harvard 11 Plus, Harvard Apparatus. Once the desired amount of discontinuous phase had passed through the membrane, both the pump and the agitator were switched off, the droplets were collected and analyzed. The agitator was driven by a 24V DC motor and paddle rotation speed was controlled by the applied voltage. Stirrer speed settings ranging from 205 to 1144 rpm (i.e. from 0.5 to 9 Pa shear stress at the membrane surface) were used. To evaluate the drop-size distribution and droplet diameter, a Malvern Mastersizer Model S (Malvern Instruments Ltd, UK) was used. For each emulsion, three separate samples and measurements were performed and the mean average of these is reported, but the difference between the triplicate samples was insignificant.

Results and Discussion

In this study, there was the need to cover wide range of injection rates, thus a preliminary comparison between the peristaltic and the syringe pump, used for the discontinuous phase injections, was performed. The substantial difference between these pumps is the way in which the fluid flow is induced. A peristaltic pump gives a semi-continuous and pulsing flow, whilst a syringe pump gives a more continuous and smooth injection. For both pumps the same tests were performed over a limited range of flow rates, in order to compare the resulting drop size distributions and determine if pump type had a significant influence on the results. In Figure 2 the data is presented in terms median droplet diameter and span (or CV)~~of D90; D50 and D10,~~ for the different systems described in the captions, as a function of the peak shear below the stirrer. This was previously determined to be the appropriate parameter with which to characterise the drops [6]. Figures 2(a) and 2(b) are for the membrane with pore spacing of 200 µm, covering injection rates between 1 and 8.7 ml/min. ~~The D90 is the drop diameter below which 90% of the distribution exists, the D50 is the median diameter and D10 is the drop diameter below which 10% of the distribution exists.~~ In all the figures the markers represent data obtained when using the peristaltic pump and the continuous lines (with no markers) represents the data from tests using the syringe pump. The only slight difference between the data obtained using these two pumps is at the low shear stress values, where the drop size is large. Even under these conditions the agreement between the two sets of data (syringe and peristaltic) is reasonable, mainly within 10% of each other. The same relation was found when using membrane with a pore spacing of 80 µm (results not shown).

~~Figures 2(a) and 2(b) are for the membrane with pore spacing of 200 µm, covering injection rates between 1 and 8.7 ml/min, and Figure 2(c) and 2(d) is for the~~

~~membrane with pore spacing of 80 µm, covering injection rates between 1 and 5 ml/min. In all cases the results are close, or identical, regardless of pump type. Hence, it may be concluded that for both membrane pore spacings: one likely to encourage the push off force and one where it is less likely; the injection pump is not contributing to the resulting drop size distribution~~. These tests justified using the syringe pump for the very low injection rates (less than the 1 ml/min illustrated in Figure 2) and the peristaltic pump for the much higher rates (more than the 8.7 ml/min illustrated in Figure 2) and comparing the results across the full injection rate spectrum.

Figure 2 also demonstrates the dependence of the droplet size with the shear stress. As previously shown, the droplet size decreases with the increasing shear [11,14,18,22-24]. The shear is reported as peak shear since, due to the geometry of the cell, the shear at the membrane has a maximum at the transitional radius distance, Figure 1(b), which has been shown to be the shear appropriate to correlate operating conditions with drop size [5]. The droplet size is a strong function of shear stress between 0 and 4 Pa, but less so at higher shear rates. It is noticeable that the shear stresses are low values, compared to many previously reported cross-flow membrane emulsifications, due to the relatively large drop size formed here and the smooth flat and regular membrane design, Figure 1(d). A shear value between 0.5 and 9 Pa corresponds to laminar flow in most cross-flow membrane systems [22,23]. Often in membrane emulsification literature the 'span' of a drop size distribution is quoted as a measure of the degree of uniformity of a distribution. This is based on the difference between the D90 and the D10, divided by the D50. The D90 is the drop diameter below which 90% of the distribution exists, the D50 is the median diameter and D10 is the drop

diameter below which 10% of the distribution exists.~~The spans of these distributions can be determined from the data provided in Figures 2~~. The spans~~, determined from the data in Figure 2,~~ vary from a maximum value of close to 1, to a minimum value of 0.5 (or CV = 22%) under the condition of 80 m^{-2} h^{-1} dispersed phase flux at 3.6 Pa when using a 200 µm pore distance (or 0.36 results not shown, under the conditions of 330 l m^{-2} h^{-1} dispersed phase flux at 1.7 Pa, when using the membrane with the closer together pores), ~~Figure 2(d).~~ Span values of monosized drops found in literature, for comparison, include: using an α- alumina membrane span ranges from 0.42 to 0.52, for a transmembrane pressure range of 60 kPa to 170 kPa [23], and using an SPG membrane span goes from 0.27 to 0.52 for a transmembrane pressure range of 1.9 Pa to 5.7 Pa [24,25].

Formatted: Font: Not Bold

200 µm pore spaced membrane

The presence of a push-off force in membrane emulsification has already been noted in the literature [8, 10, 18]. It was reported that, increasing the flux of dispersed phase, the droplet diameter increases up to a point where the droplet formation at one pore is affected by the presence of other droplets forming at the adjacent pores. This causes the droplets to detach sooner at high dispersed phase injection rates, resulting in smaller diameter and more uniform droplets size. Figures 3 and 4 show the influence of the dispersed phase flux on the droplet size in the range between 30 and 2640 l m^{-2} h^{-1} for the membrane with the higher pore spacing. The shear stress at the membrane surface was respectively 3.6 and 9 Pa, and the pore spacing was 200 µm. The distance between D10 and D90 gives an indication of span value. Figures 3 and 4 show that D90 and D10 are very close at low injections and high agitation speed, a sign of a narrow droplet size distribution, but the difference between D90 and D10 increases

with injection rate and the drop median size continues to increase with flux rate. Moreover, comparing Figures 3 and 4 it is possible to see that the drop diameter obtained at shear stress of 9 Pa is lower than the drop diameter obtained with 3.6 Pa in agreement with the literature [2, 16] and what shown in Figure 2. Hence, in the case of the 200 micron spacing between the pores, it appears that there is no evidence to suggest that a push-off force exists, at least at the higher stirrer speeds, i.e. higher values of shear stress.

Figure 5 shows the influence of the shear stress on the membrane surface on the droplet size over the full range of the experiments. The solid curve on the figure represents the shear-capillary force model without the inclusion of the push-off force. The shear-capillary model does not recognise the dispersed phase flux rate as having a contribution to the formed drop size and it is noticeable that the experiments with increasing injection rate diverge further and further away from the model prediction. So, at very low dispersed phase flux the model is in very good agreement with the measured values for median drop size. Thus, it is possible to hypothesise that, in the absence of a significant push-off force, the shear-capillary model represents the smallest drop size that should be produced for a given set of operating conditions. However, by increasing the dispersed phase flux it is possible to increase the drop size formed. Thus, the model represents the lower limit of drop size produced and increasing the flux provides higher drop diameters, but with a decrease in the degree of uniformity of the drops; as illustrated in Figure 3 and 4.

When using a membrane of 200 μm pore spacing, the droplet size decreases when increasing the shear stress at the membrane surface because of the increase in the drag

force. The droplet size formed is primarily governed by its growth time prior to detachment, which is effectively reduced at higher shear stress. The droplet size increase with dispersed phase flux can be explained by assuming a constant drop formation time, prior to detachment [20]. Hence, the increase of discontinuous phase flux results in an increase in droplet volume prior to detachment, and the formation of larger droplets. From Figure 5 it is possible to notice that the model based on Capillary and Drag force, see equations (3) and (4), gives a good prediction droplet size for emulsion obtained at low flux, but does not account for the increase in drop size based on the constant drop formation time model.

80 µm pore spaced membrane

In contrast, when using a membrane with a much lower pore spacing, it is possible to observe a different behaviour from the one above. Figure 6(a) illustrates the drop size when using an 80 µm pore spaced membrane and discontinuous phase flux from 7 to 1980 l m^{-2} h^{-1}. At low stirrer speed, 2 Volts equal to 0.5 Pa peak shear stress, there is a minimum difference between D90 and D10 values at a disperse phase flux of 1000 l m^{-2} h^{-1}. This behaviour contrasts strongly with that illustrated on Figure 3 and 4. In Figure 6(a) the curve assumes a butterfly shape, as described previously in [6], for a system which had no shear at the membrane surface. In Figure 6(a) either side of this optimum flux, the range between the D90 and D10 becomes larger. It is hypothesized that at this optimum flux of discontinuous phase most of the pores are active and the drops touch each other regularly and the push-off force facilitates the formation of consistent drops at the membrane surface. Beyond this flux, the natural broadening of the distribution as illustrated in Figures 3 and 4 occurs, leading to a wider size distribution. When increasing the shear stress at the membrane surface, the minimum

between D90 and D10 moves to higher flux of discontinuous phase. Figures 6(a) to 6(d) show this effect: the optimum discontinuous phase injection rate was measured as 1000 l m^{-2} h^{-1} for 0.5 Pa membrane shear stress. For shear stresses 1.2, 1.7, 3.6 Pa the optimum moves to higher values in what appears to be an increasingly higher optimum flux rate with increasing membrane shear. The quantitative analysis of the droplet diameters shows that the mean droplet diameter obtained with this membrane is dramatically and significantly smaller than the one produced from a membrane with 200 μm pore spacing, despite using the same size pore opening and whilst operating under similar shear conditions. This implies that in the case of the 80 μm pore spaced membrane, there is an additional force assisting in droplet detachment to that of simply shear. The droplet size distribution was also substantially narrower.

In Figures 6 two opposing phenomena connected with drop size and dispersed phase flux appear to be occurring, when considering the drop size with increasing dispersed phase flux. The mechanism of increasing drop size, as illustrated in Figures 3 and 4, predominates at high shear and is obvious at low injection rates in Figures 6(b) to 6(d). The mechanism of the push-off force, causing drop diameter to reduce as injection rate increases, is most evident at low shear, Figure 6(a), but appears to limit the drop size at even the higher shear rates. Both increasing the flux of discontinuous phase and increasing the shear at the surface membrane, the drop size distribution narrows significantly. For emulsions made with 1650 and 1980 l m^{-2} h^{-1} flux of oil and with a shear stress of 3.6 Pa very low span values were obtained (span=0.19), as can be seen in Figures 6(c) and 7(d). The drops formed using the 80 μm pore spaced membrane, and a range of peak shears, are illustrated in Figure 7 where microscope images are shown. The figures include a 100 μm scale bar in the bottom right hand

corner of each image, and the drop sizes and uniformity appear to be in line with the results provided by the Malvern Mastersizer.

Figure 8 illustrates the data obtained with the 80 μm pore spaced membrane, as both functions of peak shear stress at the membrane surface and increasing dispersed phase injection rate. The drop diameters show evidence of a strong dependency on the shear stress at the membrane surface when the injection rate is low: drop diameter decreasing with increasing shear stress. Also, at 0.5 Pa shear stress, the drop size steadily decreases with increasing flux, a consequence of push-off occurring. At 1.2 and 1.7 Pa, the drop size initially increases, but after reaching a maximum drop size, it decreases with a further increase in flux. It appears that the behaviour at 1.2 and 1.7 Pa is different than that at 3.6 Pa, where no decrease in size with flux rate is observed, but this could be because the maximum has not yet been reached when operating at this higher shear stress. Figure 8 shows that the effect of push-off force on the median drop size becomes less and less dominant, as shear stress increases from 0.5 to 3.6 Pa. At 0.5 Pa, push-off force is important from the lowest injection rate used and the drop size steadily decreases. At 1.2 and 1.7 Pa, push-off force is of minor, but increasing, importance up to the point of the maximum and becomes dominant with a further increase in flux. As a result, the drop size first increases and then decreases. At 3.6 Pa, shear force is initially dominant as compared to push-off force and drops grow with increasing injection rate. At a dispersed phase flux of around 1000 l m^{-2} h^{-1} the effect of both forces on the drop size is equally important and the drop size becomes independent of the flux. It is noticeable that at low dispersed phase flux, the experimental drop diameters tend to values obtained with the model without push-off,

whilst at high flux the experimental diameter drops tend to the diameter obtained with push-off included in the model.

At a low injection rates the capillary-shear model is assumed to be valid and at high injection rate the capillary-shear-push-off model is assumed to be more valid. Low and high injection rates are represented on the figure by the left and right hand sides of the figure. Marked at these limits are the predicted drop sizes using the two models, as indicated by bold and short horizontal lines, for each of the shear stresses used. The appropriate shear stress value for this position is also marked on the figure next to the bold line. It is noticeable that the data, at different dispersed phase fluxes, fits very well within the two limits as illustrated on Figure 8 for the low shear tests. So, for the very low injection rate the drop size with a shear of 0.5 Pa is predicted to be 220 μm, and at high injection rate the prediction is 100 μm. The measured data varies from 190 μm to 130 μm. For the highest shear stress, 3.6 Pa, the predicted drop size at low injection rate is 85 μm and the measured size at the lowest injection rate is 100 μm. At higher injection rates the observed drop size increases, for the reasons discussed above relating to constant drop formation time. However, the drop size increase slows as the push off force comes in to effect. The predicted drop size at very high injection rate, with push-off fully acting, is 80 μm, but the practical injection rate never reaches this limit. In this case, the data doesn't fit between these two limits because of the influence of drop growth with increasing injection rate – which neither model (capillary-shear or capillary-shear-push-off) recognises. However, at the limits: very low and very high injection rate, the models appear to provide a reasonable estimate of drop size, but further work is required to include the influence of injection rate – most likely based on the assumption of a fixed drop formation time.

Conclusions

Using a flat disc regular array membrane with pores 20 μm in diameter, and a simple paddle stirrer to create shear at the surface of the membrane, it has been possible to produce very monosized drops of oil in water within the range of pore spacing between 200 and 80 μm. The method for injecting oil through the hydrophilic membrane was a pump and two different types were used: a syringe pump for the very low injection rates and a peristaltic pump for the high injection rates. For a limited range of intermediate injection rates data is available for both types of pumps. There appeared to be no difference in the resulting drop size distribution, or the degree to which the drops could be described as monosized using either pump. This is a surprising result, as it is commonly believed that the dispersed phase in membrane emulsification should be injected using a smooth non-pulsing method such as a pressurised vessel, or syringe pump. A peristaltic pump is not normally recommended for this duty, as they inherently pulse the liquid flow.

The effect of the push-off force to assist in the detachment of drops from the membrane surface, together with shear at the membrane surface was studied. Using the 200 μm pore spaced membrane, the droplet size increased with the injection rate and decreased with the agitation speed (surface shear at the membrane). Monosize emulsions were only obtained at low flux. Using the 80 μm pore spacing membrane and low agitation speed, and plotting the D90, D50 and D10, as a function of injection rate, a butterfly shaped plot was obtained characterized by a point at which the drop size distribution was at its narrowest; i.e. the most monosized drops were formed away from low injection flux rates. Moving to higher agitation speeds, the minimum

moves towards higher injections rates. At low shear stress, it is noticed that an increase in discontinuous phase flux, gives rise to a decrease in the droplet size. This effect is due to the push-off force, which for the purpose of drop size modelling is added to the shear-drag and opposes the capillary force during the detachment phase, and it is an important effect in the force balance under these conditions. This effect is dominant at the membrane surface at low shear stress, with a short distance between the membrane pores, and depends on the interaction of the drops when they are formed, provided there is an absence of droplet coalescence.

The membrane with a large distance between the pores, 200 μm, showed little push-off effect, and the capillary-shear model reliably predicted the drop size at low dispersed phase injection rates. At increasing rates the drop size increased, which the literature suggests is a consequence of a constant drop formation time; hence larger drops are formed at higher injection rates. Thus, the capillary-shear model may be regarded as predicting the lower limit for drop size under these conditions and measured drop size may be greater. For the membrane with a shorter distance between the pores, 20 μm, the capillary-shear-push-off force model appeared to predict the drop size, or at least the measured drop sizes were tending towards the predicted values at very high injection rates. However, there was still a very significant influence on the measured drop sizes by the size increasing with dispersed phase injection rate.

This study illustrates some of the different mechanisms and phenomena taking place during membrane emulsification and shows that under certain circumstances drop size will increase with dispersed phase flux, whereas under other circumstances drop size

may reduce. It is possible to explain these trends of drop size and to reasonably accurately model the values under conditions of low injection rate and, arguably, very high injection rate. It is possible that the push-off force has not received much attention before as the phenomena is more prevalent on regular pore spaced membranes, which have only recently become available, than when using the matrix type of membranes, such as ceramic and SPG types. When using the latter membrane types the injected flux rate is usually very significantly less than with the regular pore spaced membranes. Hence, the likelihood of encountering push-off conditions is increasing as regular pore spaced membranes become more common.

References

(1) Lambrich, U. and Schubert, H., **2005**. Emulsification using microporous systems. *J. Membr. Sci*., 257, 76-84.

(2) Joscelyne, S.M. and Tragardh, G., **2000**. Membrane emulsification- a literature review. *J. Membr. Sci*., 169, 107-117.

(3) Nakashima, T., Shimizu, M. and Kukizaki, M., **2000**. Particle control of emulsion by membrane emulsification and its application. *Adv. Drug Del. Rev.*, 45,47-56.

(4) Van der Graaf, S., Schroën, C.G.P.H., van der Sman, R.G.M. and Boom, R.M., **2004**. Influence of dynamic interfacial tension on droplet formation during membrane emulsification. *J. Colloid Interf. Sci.*, 277,456-463.

(5) Kosvintsev, S.R., Gasparini, G., Holdich, R.G., Cumming, I.W. and Stillwell, M.T., **2005**. Liquid-liquid membrane dispersion in a stirred cell with and without controlled shear. *Ind. Eng. Chem.*, 44, 9323-9330.

(6) Stillwell, M.T., Holdich, R.G., Kosvintsev, S.R., Gasparini, G. and Cumming, I.W., **2007**. Stirred cell membrane emulsification and factors influencing dispersion drop size and uniformity. *Ind. Eng. Che. Res.*, 46, 965-972.

(7) Kosvintsev, S.R., Gasparini, G. and Holdich, R.G., **2008**. Membrane emulsification: droplet size and uniformity in the absence of surface shear. *J. Membr. Sci.*, in press.

(8) Vladisavljević, G.T. and Williams, R.A., **2006**. Manufacture of large uniform droplets using rotating membrane emulsification. *J. Colloid Interface Sci.*, 299, 396-402.

(9) Zhu, J. and Barrow, D., **2005**. Analysis of droplet size during crossflow membrane emulsification using stationary and vibrating micromachined silicon nitride membrane. *J. Membr. Sci.*, 261, 136-144.

(10) Sugiura, S., Nakajima, M., Kumazava, N., Iwamoto, S. and Seki, M., **2002**. Characterization of spontaneous transformation-based droplet formation during microchannel emulsification. *J. Phys. Chem.*, 106, 9405-9409.

(11) Rayner, M., Trägårdh, G., Trägårdh, C. and Dejmek, P., **2004**. Using the surface evolver to model droplet formation processes in membrane emulsification. *J. Colloid Interface Sci.*, 279, 175-185.

(12) Rayner, M., Trägårdh, G. and Trägårdh, C., **2005**. The impact of mass transfer and interfacial expansion rate on droplet size in membrane emulsification processes. *Colloids Surf. A*, 266, 1-17.

(13) De Luca, G., Di Maio, F.P., Di Renzo A. and Orioli E., **2007**. Droplet detachment in cross flow membrane emulsification: comparison among torque- and force-based models. *Chem. Eng. Process.*, in press, available on-line: doi:10.1016/j.cep.2007.03.010.

(14) Rayner, R. and Trägårdh, G., **2002**. Membrane emulsification modelling: how can we get from characterisation to design?. *Desalination*, 145, 165-172.

(15) Peng, S.J. and Williams, R.A., **1998**. Controlled production of emulsions using a crossflow membrane – Part I: droplet formation from a single pore. *Trans. IChemE*, 76 (A), 894-901.

(16) Vladisavljević, G.T. and Schubert, H., **2003**. Influence of process parameters on droplet size distribution in SPG membrane emulsification and stability of prepared emulsion droplet. *J. Membr. Sci.*, 225, 15- 23.

(17) Vladisavljević, G.T., Kobayashi, I., Nakajima, M., Williams, R.A., Shimizu, M. and Nakashima, T., **2007**. Shirasu porous glass membrane emulsification: characterisation of membrane structure by high- resolution x-ray microtomography and microscopic observation of droplet formation in real time. *J. Membr. Sci.*, 302, 243-253.

(18) Abrahamse, A.J., van Lierop, R., van der Sman, R.G.M., van der Padt, A. and Boom, R.M., **2002**. Analysis of droplet formation and interactions during cross-flow membrane emulsification. *J. Membr. Sci* , 204, 125-137.

(19) Schröder, V., Behrend, O. and Schubert, H., **1998**. Effect of dynamic interfacial tension on the emulsification process using microporous, ceramic membranes. *J. Colloid Interface Sci.*, 202, 334-340.

(20) Xu, J.H., Luo, G.S., Chen, G.G. and Wang, J.D., **2005**. Experimental and theoretical approaches on droplet formation from a micrometer screen hole. *J. Membr. Sci.*, 266, 121-131.

(21) Keh, H.J. and Chen, P.Y., **2001**. Slow motion of a droplet between two parallel plane walls. *Chem. Eng. Sci.*, 56, 6863-6871.

(22) Schröder, V. and Schubert, H., **1999**. Production of emulsions using microporous, ceramic membranes. *Colloid Surf. A*, 152, 103-109.

(23) Vladisavljević, G.T. and Schubert, H., 2**003**. Preparation of emulsions with a narrow particle size distribution using microporous α-alumina membranes. *J. Disper. Sci. Technol.*, Vol 24, N.6, 811-819.

(24) Vladisavljević, G.T. and Schubert, H., 2**003**. Influence of process parameters on droplet size distribution in SPG membrane emulsification and stability of prepared emulsion droplets. *J. Membr. Sci.*, 225, 15-23.

(25) Vladisavljević, G.T., Lambrich, U., Nakajima, M. and Schubert, H., **2004**. Production of O/W emulsions using SPG membranes, ceramic α-aluminium oxide membranes, microfluidizer and a silicon microchannel plate-a comparative study. *Colloid Surf. A*, 232, 199-207.

List of Figures

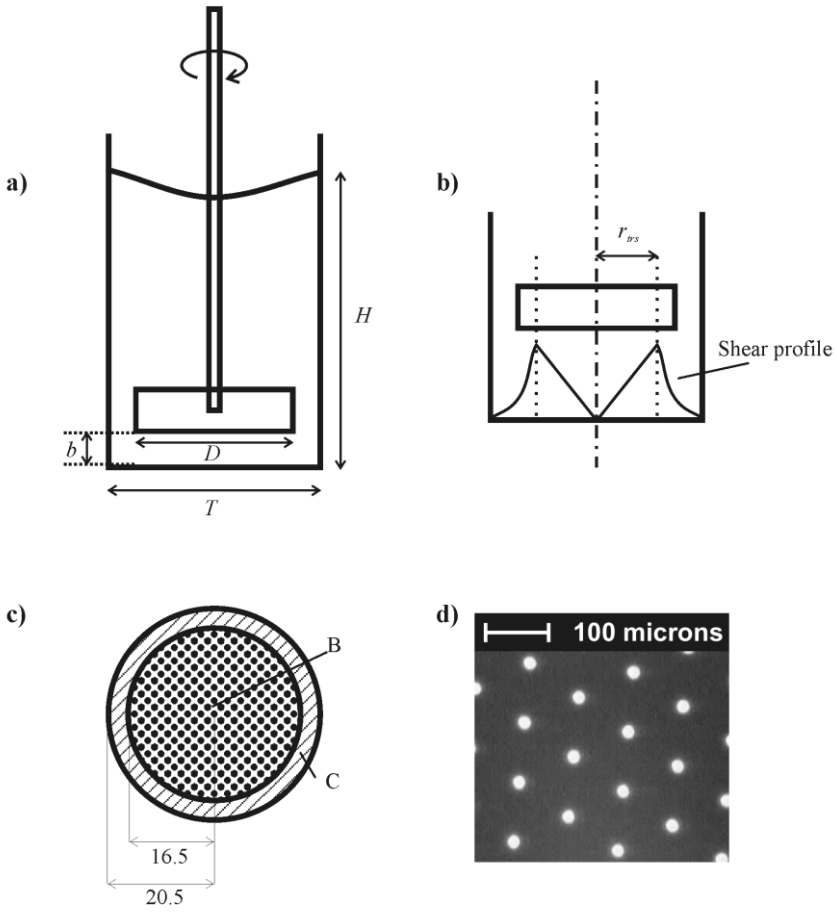

Figure 1 Schematic illustration of experimental apparatus and membrane used: a) Dispersion Cell with simple paddle, b) shear profile below rotating paddle, c) dimensions of membrane used at the base of the cell, d) microscope picture of the regular pore array membrane used

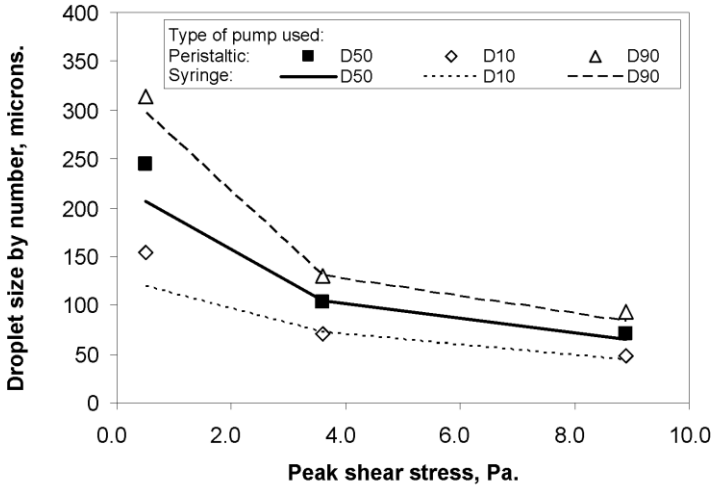

Figure 2 (a) Comparison of injection pump type used for dispersed phase: (a) membrane pore spacing 200 μm, injection rate 1 ml/min

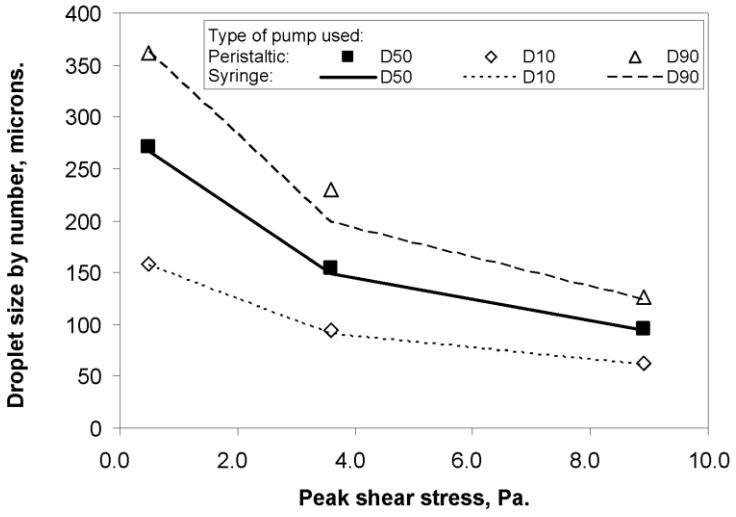

Figure 2(b) Comparison of injection pump type used for dispersed phase:
(b) membrane pore spacing 200 μm, injection rate 8.7 ml/min

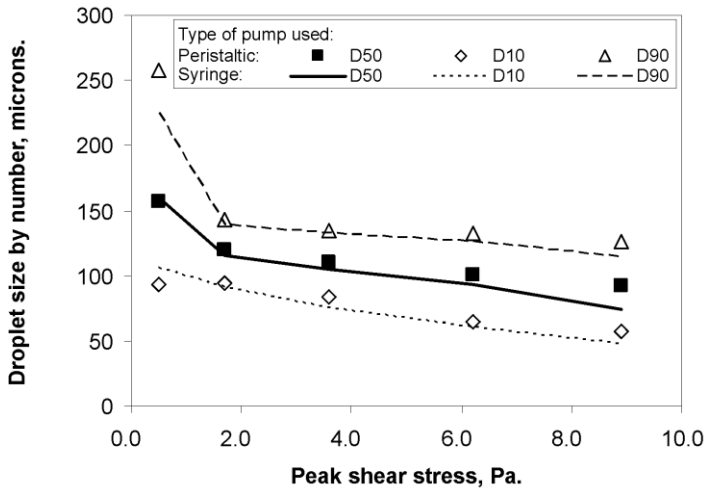

Figure 2(c) Comparison of injection pump type used for dispersed phase: (c) membrane pore spacing 80 μm, injection rate 1 ml/min

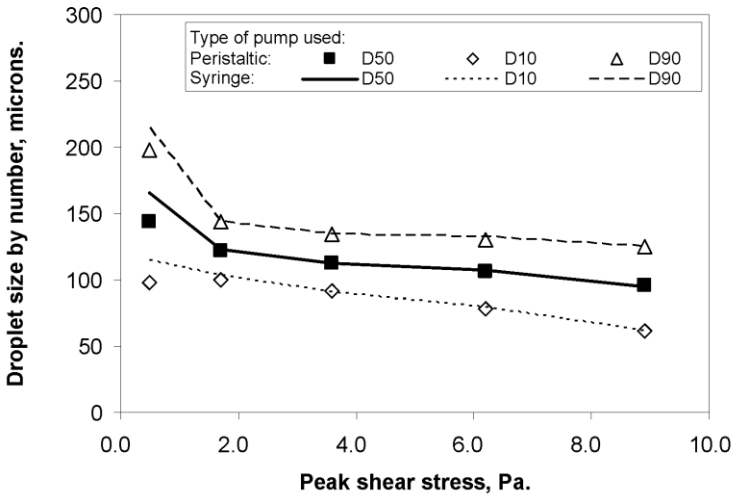

Figure 2(d) Comparison of injection pump type used for dispersed phase: (d) membrane pore spacing 80 μm, injection rate 5 ml/min

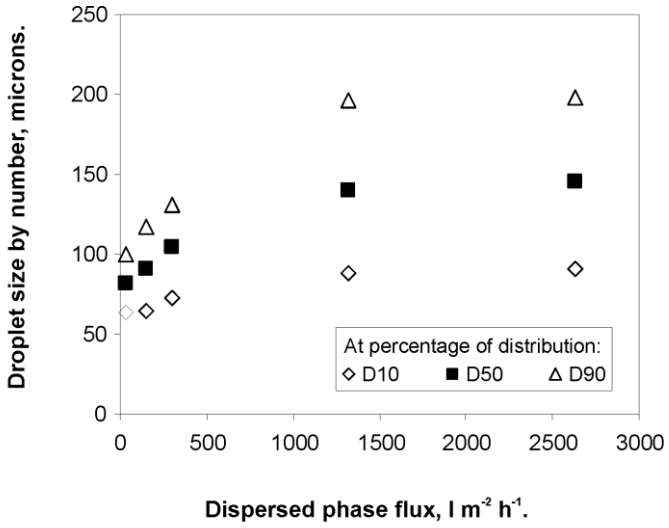

Figure 3 Variation of droplet size and distribution with injection rate for 200 micron pore spacing membrane and 6 Volts (650 rpm) agitation – 3.6 Pa peak shear at membrane

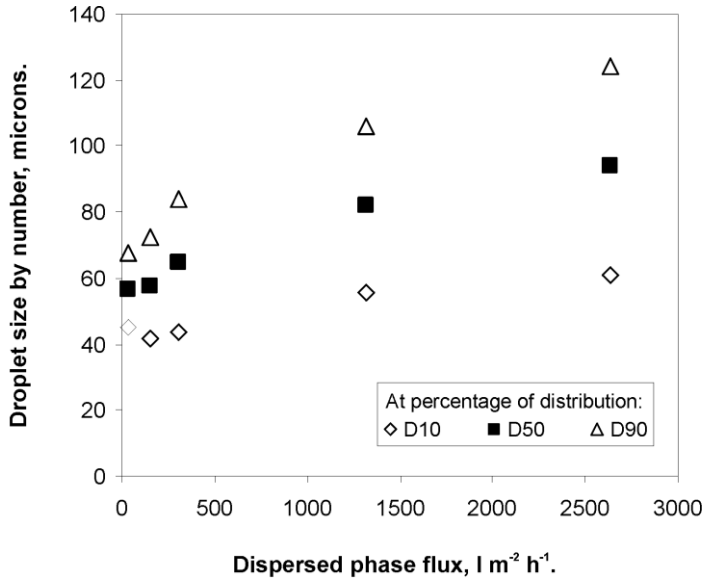

Figure 4 Variation of droplet size and distribution with injection rate for 200 μm pore spacing membrane and 10 Volts (1150 rpm) agitation– 8.9 Pa peak shear at membrane

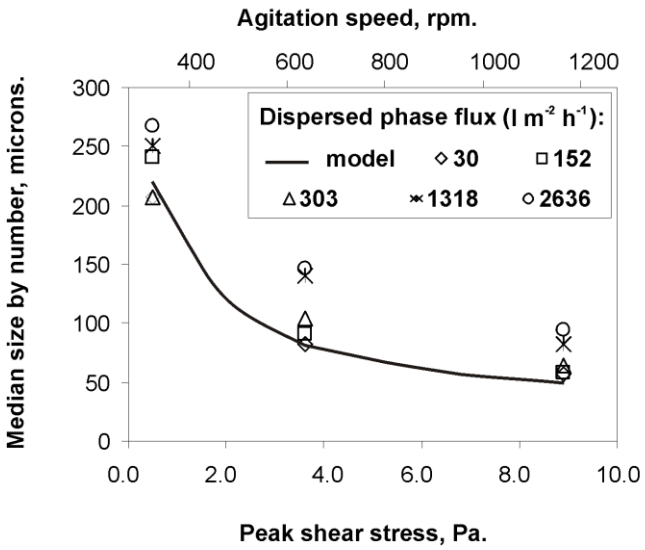

Figure 5 Comparison of measured median drop size with shear-capillary force model for 200 μm pore spaced membrane at various agitation rates

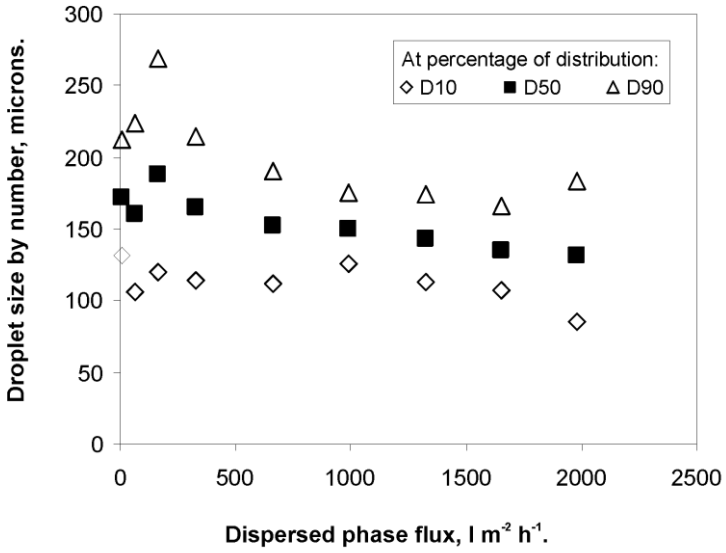

Figure 6(a) Variation of droplet size and distribution with injection rate for 80 μm pore spacing membrane and:
(a) 2 Volts (210 rpm) agitation– 0.5 Pa peak shear at membrane

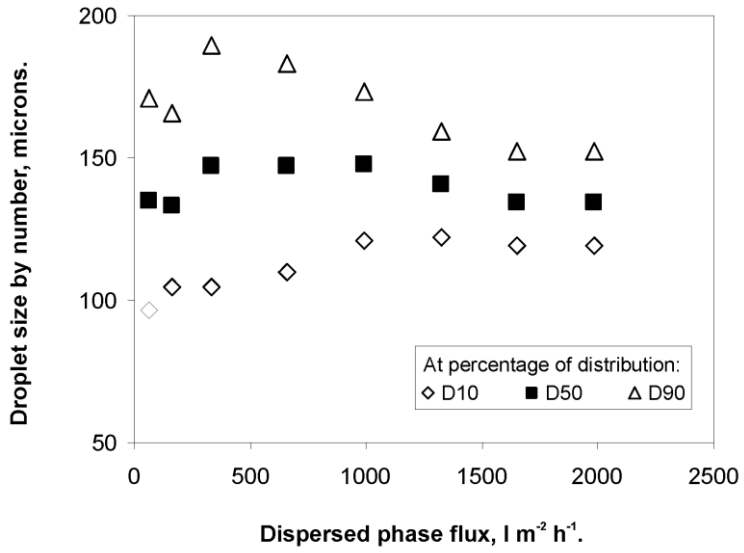

Figure 6(b) Variation of droplet size and distribution with injection rate for 80 μm pore spacing membrane and:
(b) 3 Volts (340 rpm) agitation – 1.2 Pa peak shear at membrane

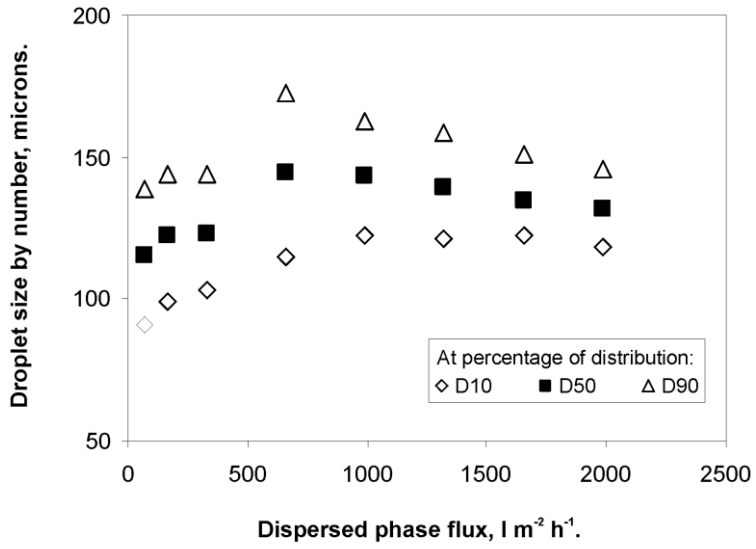

Figure 6(c) Variation of droplet size and distribution with injection rate for 80 μm pore spacing membrane and:
(c) 4 Volts (410 rpm) agitation – 1.7 Pa peak shear at membrane

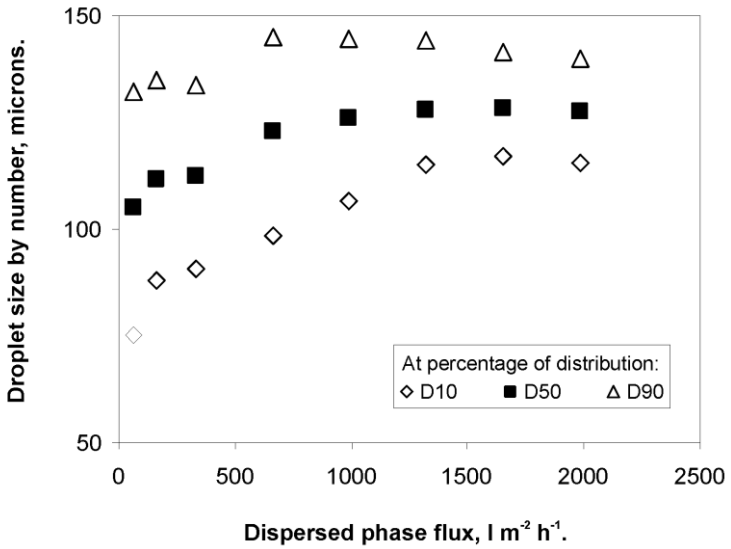

Figure 6(d) Variation of droplet size and distribution with injection rate for 80 μm pore spacing membrane and:
(d) 6 Volts (650 rpm) agitation – 3.6 Pa peak shear at membrane

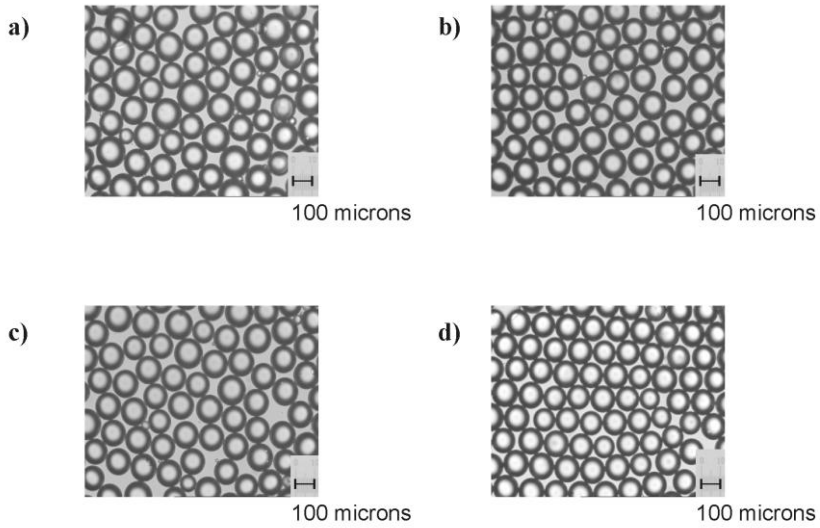

Figure 7 Optical microscope images of drops formed with 80 μm pore spacing membrane and:
(a) 2 Volts agitation (210 rpm) – 0.5 Pa peak shear at membrane
(b) 3 Volts agitation (340 rpm) – 1.2 Pa peak shear at membrane
(c) 4 Volts agitation (410 rpm) – 1.7 Pa peak shear at membrane
(d) 6 Volts agitation (650 rpm) – 3.6 Pa peak shear at membrane

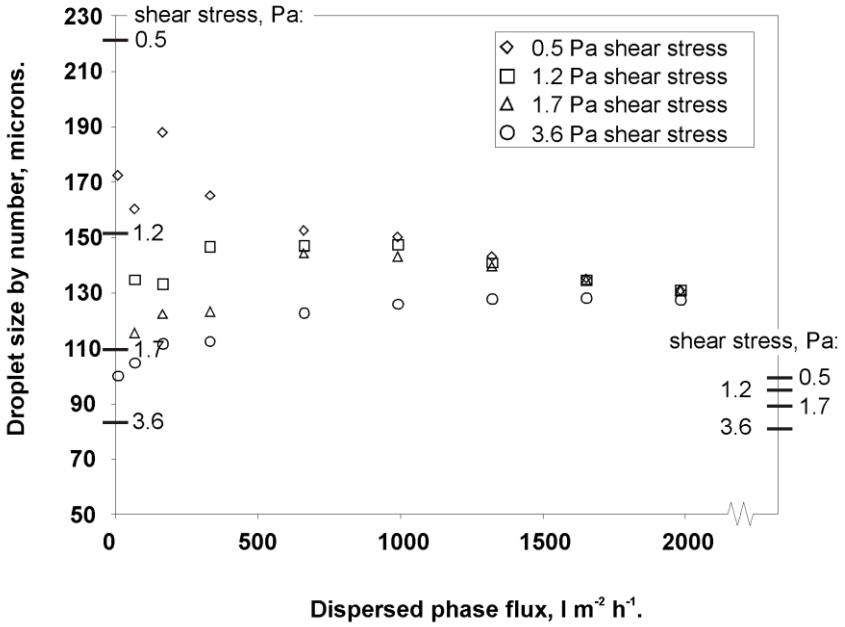

Figure 8 Measured median drop sizes with injection rate for 80 μm pore spacing membrane and marked shear rates – with limits provided by the two predictive models